Electronic Supplementary Material (ESI) for Sustainable Energy & Fuels.

Facile Preparation of Nickel Hydroxide Nanoplates Grown on Nickel Foam for High Performance of Hydrogen Generation

Jun Cao[a], Zejie Zhang[a], Haichao Li[a], Ruitong Zhu[a], Songbo Li[b], Li Ma[a], Kechao Zhou[a], Qiuping Wei[b, *], Fenghua Luo[a, *]

[a] State Key Laboratory of Powder Metallurgy, Central South University, Changsha, Hunan, 932 Lushan South Road, 410083, PR China.

[b] School of Materials Science and Engineering, Central South University, Changsha, Hunan, 932 Lushan South Road, 410083, PR China.

[*] E-mail: **fenghualuo@csu.edu.cn (F. H. Luo); qiupwei@csu.edu.cn (Q. P. Wei)**

1. Experimental sections

1.1. Materials

Nitric acid (A.R) was bought from Hunan Huihong reagent Co. LTD. Ni foam (110 ppi) was bought from Suzhou Jiashide Foam Metal Co.Ltd. The pure water was produced from the ultra-pure purification system (UPC-1-10T).

1.2. The preparation of $Ni(OH)_2$ on Ni foam

A piece of NF (1 cm ×1.5 cm) was successively washed by acetone, 3 M HCl, and deionized water for 15 minutes. Then, NF was putted into a glass bottle containing 10 mL HNO_3 solution (0.1 M) and the bottle was putted in an electro-thermostatic water bath keeping at 80 °C for 4 hours. Then, NF was removed from solution and rinsed by pure water. Finally, NF was dried at 60 °C for 2 h.

1.3. Characterization

The X-ray diffraction and Raman spectroscopy of samples were obtained in D/max-2500VB (Rigaku Corporation) and LabRAM HR800 (HORIBA), respectively. The micromorphology was investigated by scanning electron microscopy (SEM, FEI Quanta 250 and Tescan Mira3) and transmission electron microscopy (TEM, FEI Tecani G2 F20). The X-ray photoelectron spectroscopy (XPS) was collected in Thermo Fisher-VG Scientific 250XI. The Raman spectra were determined by LabRAM HR800.

1.4. Electrochemical Test

The electrochemical tests were conducted at an electrochemical station with a three-electrode system (CHI660E) in 1.0 M KOH solution. A piece of NF (1.5 cm × 0.5 cm, exposed area 0.5 cm^2), graphite rod, and Hg/HgO were regarded as working, auxiliary, and reference electrodes, respectively. All measured potentials were calibrated to reverse hydrogen electrode (RHE) according to a previous method[1]:

$$E(RHE) = E(Hg/HgO) + 0.926\ V \qquad (1)$$

The LSV curves were obtained at a scan rate of 5 mV s^{-1} after cyclic voltammetry (CV) scanning and they were corrected by *iR* compensation, where *R* value was solution resistance in equivalent circuit. The double layer capacitance (C_{dl}) was determined by the CV curves recorded between 0.052 V and 0.252 V at variable scan rates. The C_{dl} was the half value of the slope by plotting the current density differences at 0.152 V against the scan rates. The electrochemical impedance spectroscopy (EIS) was performed at -98 mV between 10^5 Hz and 0.05 Hz and the disturbance in each test is 5 mV.

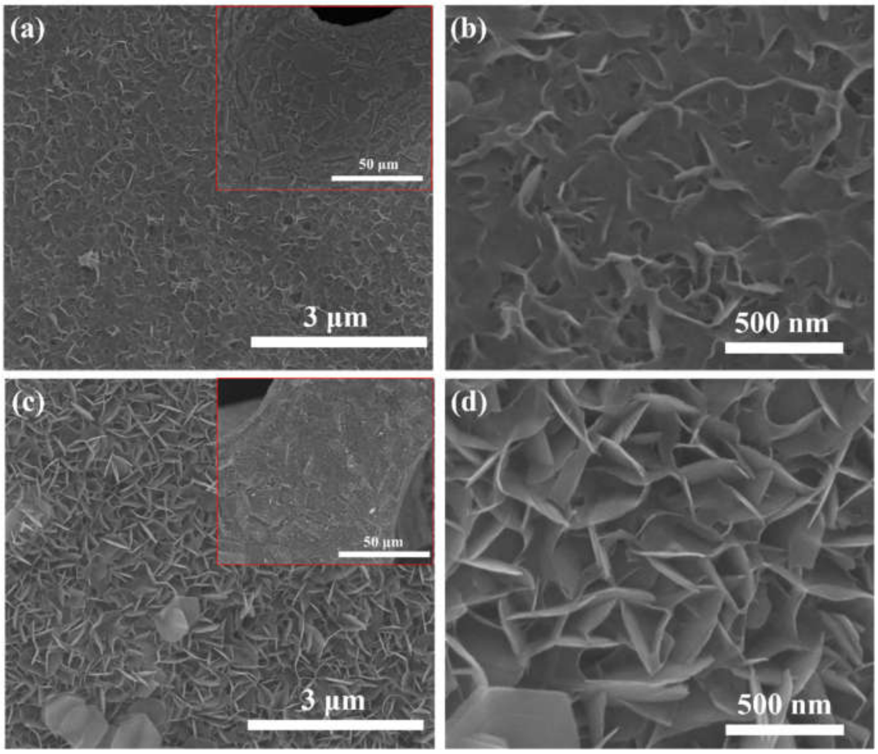

Fig. S1 SEM images of nickel foam treated in different temperature: (a and b) 60 ℃, (c and d) 70 ℃. The insets in a and c are the low magnifications of individual sample.

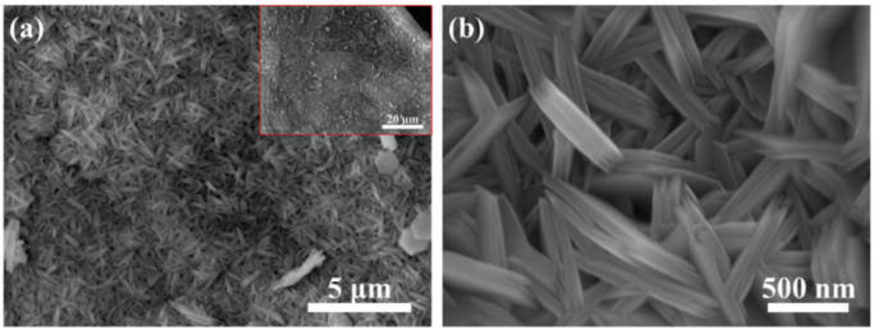

Fig. S2 SEM images of nickel foam treated in different temperature: (a and b) 90 ℃ for 4 h. The insets in a is the low magnifications of the sample.

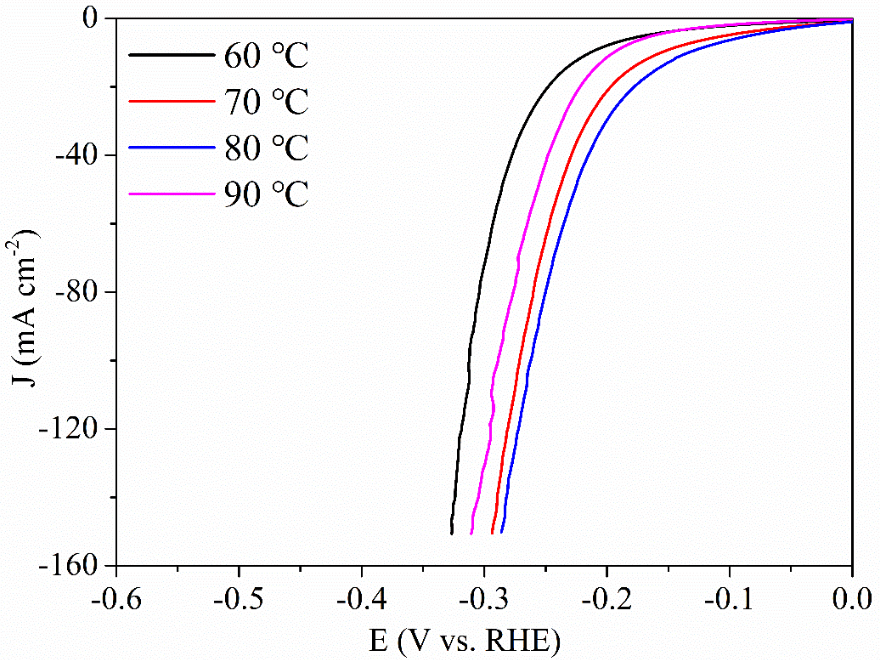

Fig. S3 The LSV comparison of the electrodes obtained at 4 h under different reaction temperature.

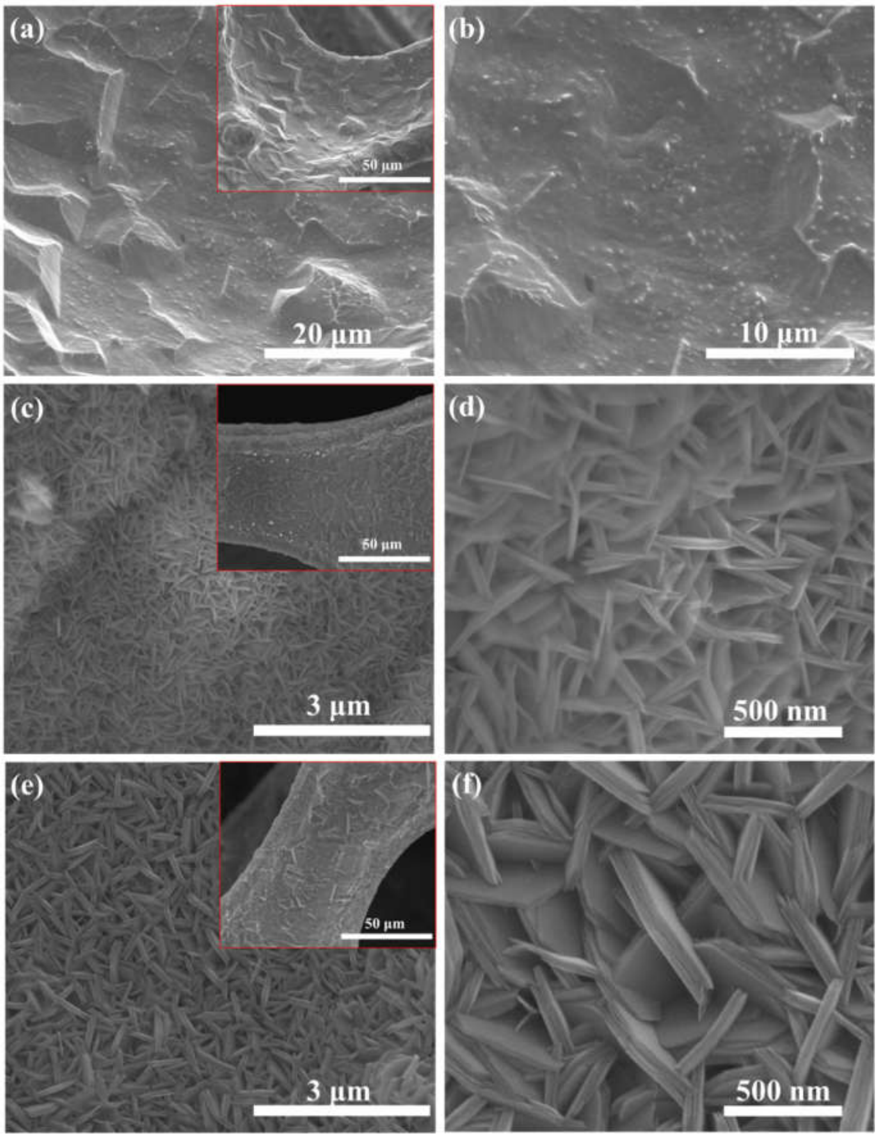

Fig. S4 SEM images of samples treated under 80 °C for different time: (a-b) 1 h; (c-d) 2 h; (e-f) 6 h. The insets in a, c, and e are the low magnifications of individual sample.

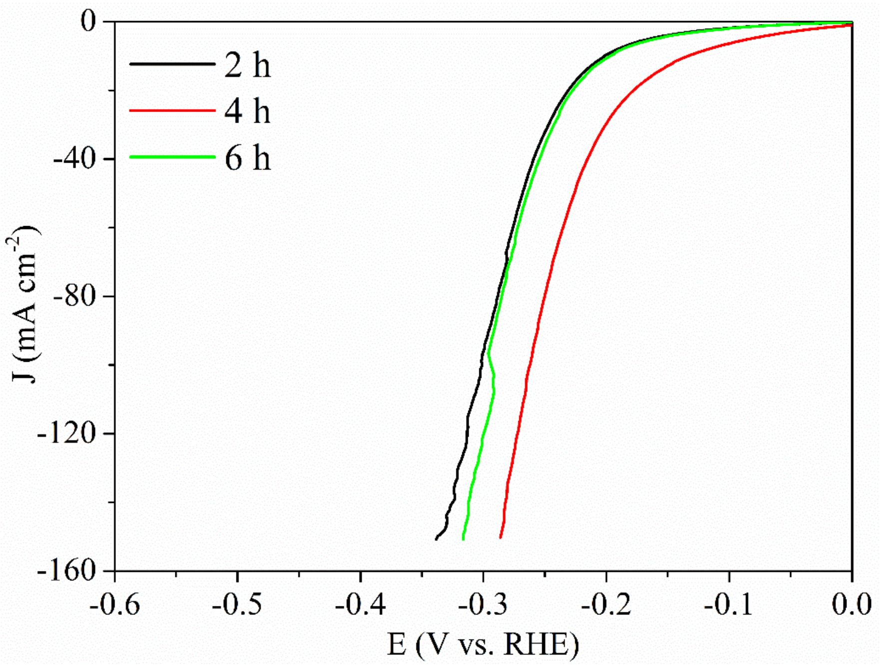

Fig. S5 The LSV comparison of the electrodes obtained under 80 °C for different reaction temperature.

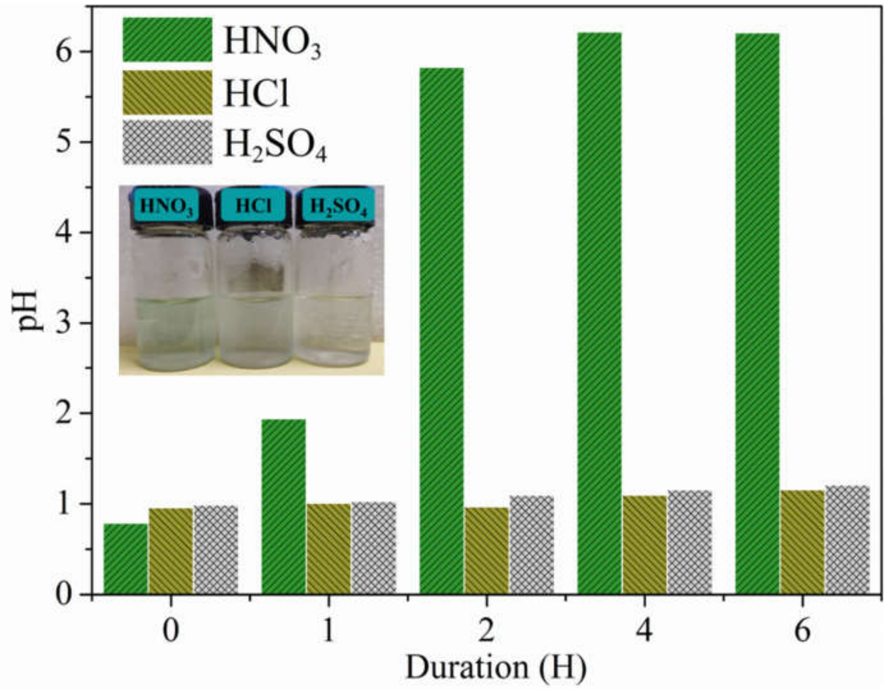

Fig. S6 pH value changes of the acid solutions under 80 ℃ at different time (the inset is the photography of solution after 6 h treatment).

When NF is soaked in HNO_3 solution, pH value of the solution is gradually increased with the increase of soaking time. Meanwhile, the solution is changed to light green after 6 h treatment. However, pH of HCl and H_2SO_4 remain at about 1 during 6 h treatment and the solutions are almost colorless after treating 6 h. Such result indicates that the amount of Ni corroded by HCl or H_2SO_4 is far less than that corroded by HNO_3. Moreover, the low pH value of HCl and H_2SO_4 after reaction is detrimental to $Ni(OH)_2$ precipitation. Therefore, comparing to HCl and H_2SO_4, HNO_3 is facilitated to the faster formation of $Ni(OH)_2$ at the same time period.

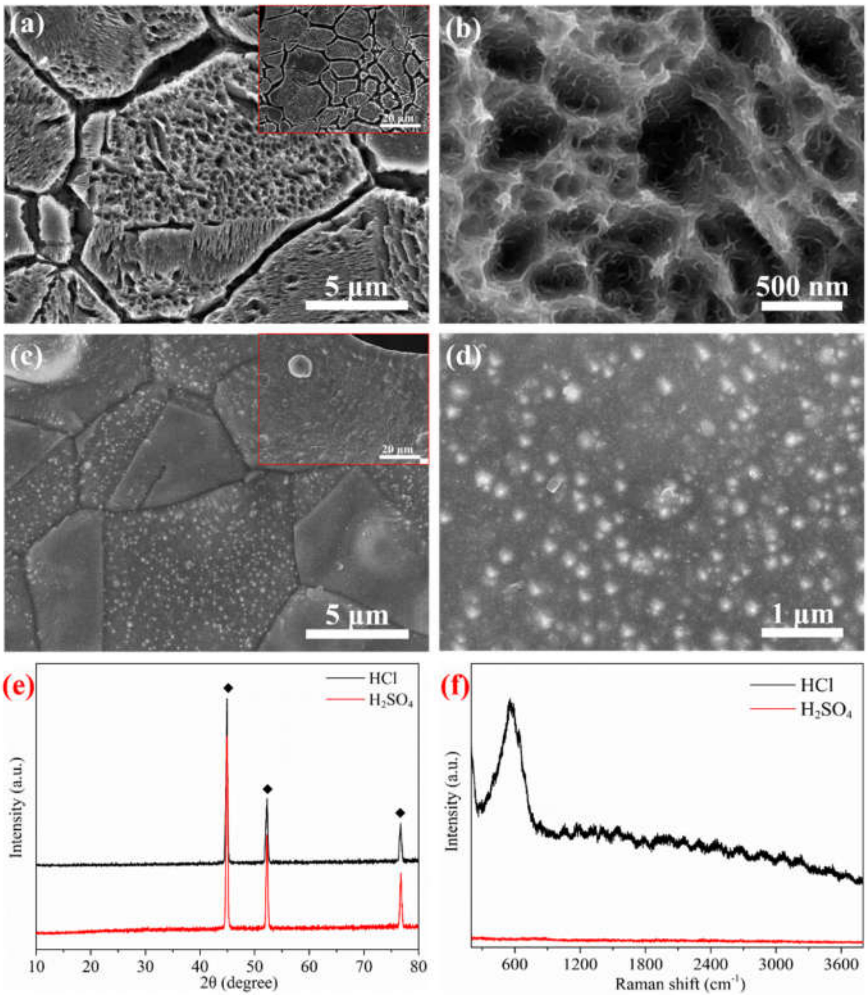

Fig. S7 The morphology characterization of NF treated in different acid solution under 80 °C for 4 h: (a-b) HCl, (c-d) H_2SO_4; The phase and composition characterization of the corresponding products: (e) XRD pattern (◆ represents NF), (f) Raman spectroscopy.

HCl and H_2SO_4 are applied instead of HNO_3 to corrode nickel foam. It is observed that the surface of NF treated in HCl is cracking-field-like morphologies with the cracks along the grain boundaries (Fig. S7a). From the magnified image (Fig. S7b), there are many pitting holes and tiny nanosheets on the surface of grain. The same result was observed in previous report[2, 3]. Moreover, the use of H_2SO_4 produce some corrosion heritages (Fig. S7c) and some "apophyses" (Fig. S7d) on the surface. Moreover, the NF treated in HCl and H_2SO_4

is further characterized by XRD and Raman. Besides the peaks of NF, there are other peaks presented in the XRD pattern (Fig. S7e), indicating that there are no products on the surface of NF or the amounts of products are less than the limitation of instrument. The Raman spectroscopy shows that NF processed in HCl solution possesses one peak located in 533 cm^{-1}, which is ascribed to Ni-O bond of NiO[4]. However, there are no peaks appeared in the spectroscopy of NF processed in H_2SO_4. Therefore, the products after soaking in HCl and H_2SO_4 are NiO and Ni. Such results reveal that $Ni(OH)_2$ with nanoplates cannot be directly obtained by treating nickel foam under HCl and H_2SO_4 in short time. However, there were some works reported that $Ni(OH)_2$ can be formed on nickel under HCl and H_2SO_4 while it needed fierce conditions of high temperature, high pressure, and long reaction time[5, 6].

In our work, the $Ni(OH)_2$ can be produced by using HNO_3 to treat NF under low temperature for short time. This is ascribed to the corrosion capability of HNO_3 is higher than that HCl and H_2SO_4[7], which is facilitated to the faster formation of $Ni(OH)_2$ at the same time period. Certainly, the exact mechanism is not yet fully understood and requires further study.

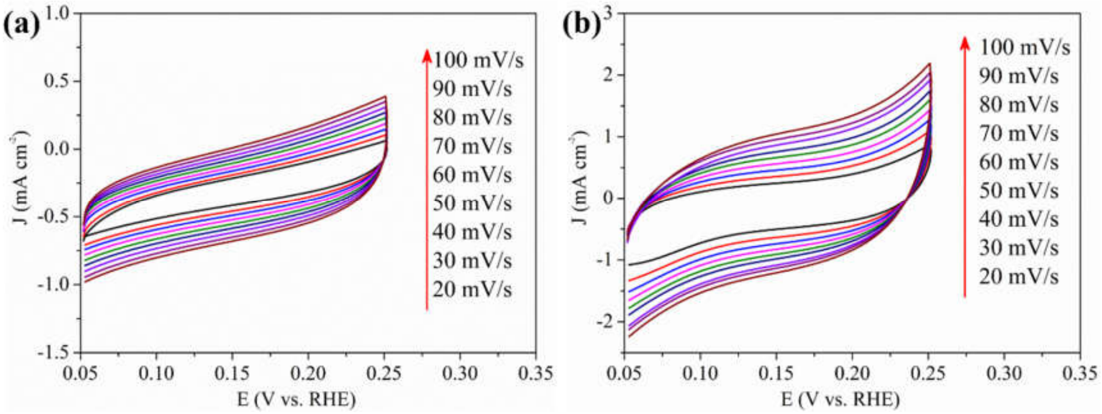

Fig. S8 The CV curves of various electrodes at different scan rates: (a) NF, (b) $Ni(OH)_2$/NF.

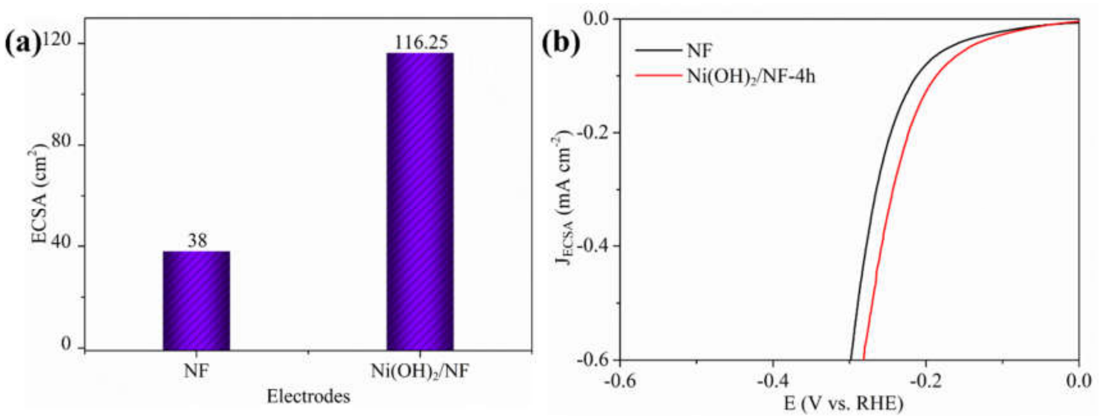

Fig. S9 (a) The ECSA comparison of the two electrodes. (b) The polarization curves of the different electrodes based on ECSA.

The electrochemical surface area (ECSA) was estimated from the electrochemical double layer capacitance. The calculation equation is as follows.

$$A_{ECSA} = \frac{\text{specific capacitance}}{40\ \mu F\ cm^{-2}} \times A_{geom}$$

Where specific capacitance is C_{dl} (Fig. 4c and Fig. R1b); 40 μF cm^{-2} is the specific capacitance of a flat surface[8]; A_{geom} is the area of working electrode (0.5 cm^2 for NF and $Ni(OH)_2$/NF).

$$A_{ECSA}\ (NF) = \frac{3.04\ \text{mF}\ cm^{-2}}{40\ \mu F\ cm^{-2}} \times 0.5\ cm^2 = 38\ cm^2$$

$$A_{ECSA}\ (Ni(OH)_2/NF) = \frac{9.3\ \text{mF}\ cm^{-2}}{40\ \mu F\ cm^{-2}} \times 0.5\ cm^2 = 116.25\ cm^2$$

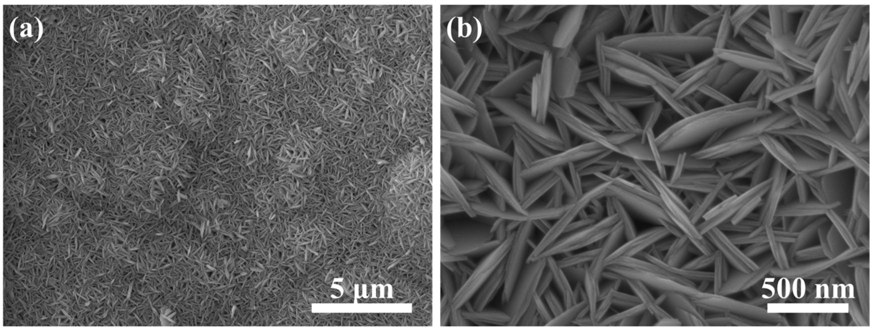

Fig. S10 The low (a) and high resolution (b) of SEM images of $Ni(OH)_2$/NF after stability test.

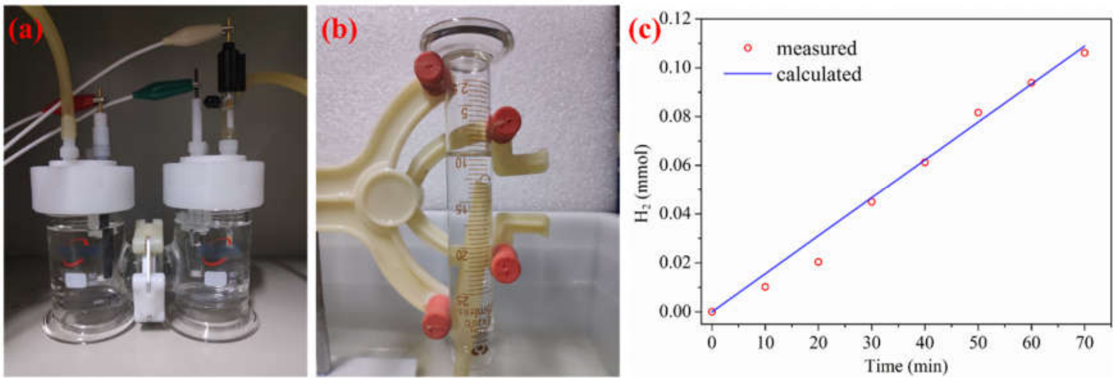

Fig. S11 (a) The digital image of H-type electrolyzer; (b) The volume of produced H_2; (c) Amounts of measured and calculated H_2.

The Faradaic efficiency (FE) is calculated based on the following formula[9, 10]:

$FE = (V/V_m)/(Q/(n\times F)$

In where, V is the volume of gas evolved during test. V_m is the molar volume (22.4 L mol^{-1}, 298 K), Q is total quantity of electric charge (C), *F* is the Faradic constant (96485.3 C mol^{-1}) and n is the number of moles of electrons transferred during the reaction while it is generating 1 mol for gas (which is 2 for H_2).

By comparing the amount of theoretically calculated H_2 with the experimentally measured quantities, it was found that the faradic efficiency is 98%, which is close to 100%, indicating that the electrocatalytic reaction is performed with high energy-conversion rate and efficiency.

Table S1 Comparison of the HER performance of NF-80°C-4h with previously reported Ni-based and $Ni(OH)_2$-based electrocatalysts.

Catalysts	Solution	Overpotential (mV) η@10 mA/cm^2	Reference
NF-80°C-4h	1.0 M KOH	131	**This work**
Ni	1.0 M KOH	164	11
$Ni(OH)_2$/NF	1.0 M KOH	127	12
$Ni(OH)_2$	1.0 M KOH	~ 310	13
CNC Pt-Mn/$Ni(OH)_2$	0.1 M KOH	~ 200	14
$Ni(OH)_2$+CuS	1.0 M KOH	186	15
Ni/NF	1.0 M KOH	173	16
NiCo-OH/NF	1.0 M KOH	201	17
Ni@$Ni(OH)_2$	1.0 M KOH	345	18
1st-Ni/$Ni(OH)_2$/NF-500	1.0 M KOH	116	19
Fe-$Ni(OH)_2$/NF	1.0 M KOH	160	20

References

1. S. M. Unni, G. M. Anilkumar, M. Matsumoto, T. Tamaki, H. Imai and T. Yamaguchi, *Sustainable Energy & Fuels*, 2017, **1**, 1524-1532.
2. H. Sun, Z. Ma, Y. Qiu, H. Liu and G. Gao, *Small*, 2018, DOI: 10.1002/smll.201800294, 1800294.
3. M. Yu, W. Wang, C. Li, T. Zhai, X. Lu and Y. Tong, *NPG Asia Materials*, 2014, **6**, 129.
4. P. E. Saranya and S. Selladurai, *New J Chem*, 2019, **43**, 7441-7456.
5. B. Hu, X. Qin, A. M. Asiri, K. A. Alamry, A. O. Al-Youbi and X. Sun, *Electrochimica Acta*, 2013, **107**, 339-342.
6. J. Tian, Z. Xing, Q. Chu, Q. Liu, A. M. Asiri, A. H. Qusti, A. O. Al-Youbi and X. Sun, *CrystEngComm*, 2013, **15**, 8300-8306.

7. J. Xie, P. Yin, W. Shi, M. Hu, J. Wang, X. Zhou, J. Han, S. Cao, L. Han and Y. Yao, *Journal of Wuhan University of Technology-Mater. Sci. Ed.*, 2016, **31**, 872-876.
8. C. Tang, W. Wang, A. Sun, C. Qi, D. Zhang, Z. Wu and D. Wang, *ACS Catalysis*, 2015, **5**, 6956-6963.
9. T. Bhowmik, M. K. Kundu and S. Barman, *Acs Applied Energy Materials*, 2018, **1**, 1200-1209.
10. P. W. Menezes, C. Panda, S. Loos, F. Bunschei-Bruns, C. Walter, M. Schwarze, X. Deng, H. Dau and M. Driess, *Energy & Environmental Science*, 2018, **11**, 1287-1298.
11. K. Yao, M. Zhai and Y. Ni, *Electrochimica Acta*, 2019, **301**, 87-96.
12. Y. Rao, Y. Wang, H. Ning, P. Li and M. Wu, *Acs Appl Mater Inter*, 2016, **8**, 33601-33607.
13. B. Zhang, J. Liu, J. Wang, Y. Ruan, X. Ji, K. Xu, C. Chen, H. Wan, L. Miao and J. Jiang, *Nano Energy*, 2017, **37**, 74-80.
14. Y. Wang, H. Zhuo, X. Zhang, X. Dai, K. Yu, C. Luan, L. Yu, Y. Xiao, J. Li, M. Wang and F. Gao, *Nano Energy*, 2018, **48**, 590-599.
15. S. Liu, H. Wen, G. Ying, Y. Zhu, X. Fu, R. Sun and C. Wong, *Nano Energy*, 2018, **44**, 7-14.
16. F. Song, W. Li, G. Han and Y. Sun, *ACS Applied Energy Materials*, 2017, **1**, 3-8.
17. H. Liang, A. N. Gandi, D. H. Anjum, X. Wang, U. Schwingenschlogl and H. N. Alshareef, *Nano Letters*, 2016, **16**, 7718-7725.
18. Z. Deng, J. Wang, Y. Nie and Z. Wei, *Journal of Power Sources*, 2017, **352**, 26-33.
19. Y. Liu, J. Wang, Q. Tian, M. Liu, X. Wang, P. Li, W. Li, N. Cai, W. Chen and F. Yu, *CrystEngComm*, 2019, **21**, 3431-3438.
20. J. Ren, G. Yuan, C. Weng, L. Chen and Z. Yuan, *Nanoscale*, 2018, **10**, 10620-10628.